# Quadrics for Structuring Invariant SpaceTime Wavepackets

Pierre Béjot, Bertrand Kibler

# Quadrics for structuring invariant space-time wavepackets

Pierre Béjot * and Bertrand Kibler

*Laboratoire Interdisciplinaire Carnot de Bourgogne, UMR6303 CNRS-UBFC, 21000 Dijon, France*

**Abstract:** Space-time light structuring has emerged as a very powerful tool for controlling the propagation dynamics of pulsed beam. The ability to manipulate and generate space-time distributions of light has been remarkably enhanced in past few years, letting envision applications across the entire spectrum of optics. Space-time invariant optical wavepackets manipulated up to now are usually two-dimensional objects (one space dimension and time) whose mode-resolved spectra lie in a conical section. Using simple symmetry and invariance principles, we show that such wavepackets are particular cases of more general three-dimensional structures whose space-time frequencies lie on quadric surfaces. Our proposed framework allows here classifying invariant space-time wavepackets localized in all dimensions, in any group-velocity dispersion regime, both in bulk and waveguides. Particular emphasis is placed on longitudinal orbital angular momentum-carrying space-time wavepackets. This unprecedented theoretical approach opens the way for versatile synthesizing of space-time optics.

*Corresponding author. Email address: pierre.bejot@u-bourgogne.fr

*Keywords: Space-time wavepackets; orbital angular momentum; optical waveguides; light structuring*

***Introduction.*** Symmetry and invariant principles play a fundamental role in modern physics.[1-2] Major examples from classical mechanics are the total energy, and linear and angular momenta obeying respective conservation law associated with continuous symmetries (time translation, space translation and rotation). The group theory is the prominent mathematical approach for studying symmetries in various branches ranging from solid state physics to quantum physics. It allows to analyze symmetries and their implications in a unified way for distinct physical systems, including solving or simplifying various problems, such as obtaining analytic solutions of differential equations (e.g. Lie's method). Application of symmetries in optical physics can be easily found in geometrical optics and optical aberrations,[3-4] as well as the derivation of non-diffracting solutions in free space.[5-7] For the latter, the symmetry group associated with Helmholtz equation and the coordinate systems in which variables separate give rise to various solution families of invariant or accelerating waves and beams such as plane waves, Bessel and Mathieu beams, and Weber waves.[8-10] Orbital angular momentum (OAM)-carrying beams (i.e., vortex beams) are other possible monochromatic solutions (not always diffraction-free) associated to screw axis symmetry.[11] Besides the intense research activities on optical vortex beams carrying longitudinal OAM (i.e., the spiral phase twists in the spatial domain), the recent studies on spatiotemporal optical vortices (STOVs) carrying transverse or tilted OAM (here the phase rotates in the spatiotemporal domain) have opened up new opportunities for structuring light.[12-17]

More generally, structured light, particle beams, and invariant wavepackets are nowadays indispensable tools in numerous fields of science and technology,[18-24] and a new step forward in the advanced control of wave propagation would facilitate the emergence of new functionalities. While most of the above examples have been deeply studied in the monochromatic regime, strong interest is currently shown for space-time (ST) invariant wavepackets. Among them, one can cite space-time light sheets,[25] needle pulses,[26] X- and O-waves.[27-29] Invariant STOVs have also been observed in the anomalous dispersion regime.[16] Structuring the space-time characteristics of a field turns out to be a very versatile way to engineer the pulse propagation dynamics, allowing, for instance, to control the group velocity[25,30] or group velocity dispersion,[31-32] as well as OAM features[16,33] of the structured wavepackets. Not only used for sculpting "at will" the propagation dynamics, the framework of invariant ST wavepackets has provided a deeper understanding of the mechanisms responsible for supercontinua generation during the nonlinear propagation of ultrashort pulses.[27,34-35] In a geometrical point of view, all the aforementioned studied space-time structures are two-dimensional and share the particularity to own a frequency-resolved modal decomposition that lies on a conic section. Since extremely fast progresses are currently made for generating more and more complex three-dimensional light structures,[33,36] it then seems particularly important at this point to provide an exhaustive classification of three-dimensional invariant ST wavepackets.

In the present work, we provide a general approach for structuring three-dimensional light ultrashort pulses in

both bulk and structured dispersive media. We show that, in two different space coordinates systems (Cartesian and cylindrical), ST wavepackets that are invariant under uniform rectilinear-motion and spatial rotation operations can be built from the coherent superposition of modes that lie on quadric surfaces in the frequency-resolved modal space. The nature of surfaces depends on the considered dispersion regime and the group-velocity of the wavepacket. The geometrical study of the considered quadrics then allows constructing invariant ST wavepackets propagating with arbitrarily chosen group velocity and rotation. Every invariant ST wavepackets studied so far could be investigated within a similar framework. Note that the same analysis could be performed in spherical coordinates[37] or space-time cylindrical coordinates,[16] the quest for invariant wavepackets being intertwined with symmetries of the considered medium of propagation.

***Propagation equation in the modal representation.*** The partial differential equation driving the linear propagation in bulk media of an electric field $E$ is given by:

$$[\partial_z^2 + \Delta_\perp + k^2(\omega)]\tilde{E}(\vec{r}_\perp, z, \omega) = 0, \qquad (1)$$

where $k(\omega) = \frac{n(\omega)\omega}{c}$, $c$ is the light velocity in vacuum, $n(\omega)$ is the refractive index at the angular frequency $\omega$, $\Delta_\perp$is the transverse Laplacian operator, $\vec{r}_\perp$ is the transverse position vector, and $\tilde{E}$ is the Fourier transform of $E$ with respect to the time coordinate. The very first step for studying z-invariant ST wavepackets is to express the eigenvectors (called hereafter "modes") of the operator $\square_\perp : \Delta_\perp + \frac{n^2(\omega)\omega^2}{c^2}$. In the Cartesian (resp. cylindrical) case, they simply correspond to monochromatic plane waves $e^{ik_y y}e^{ik_x x}e^{-i\omega t}$ [resp. orbital angular momentum Bessel monochromatic waves $J_l(k_\perp r)\, e^{il\theta}e^{-i\omega t}$] with eigenvalues $K_z{}^2 = k^2(\omega) - k_\perp^2$, where $k_\perp^2 = k_x^2 + k_y^2$. The evolution of a field $E$ along the $z$ direction is given by:

$$\partial_z \bar{E} = iK_z \bar{E}, \qquad (2)$$

where $\bar{E}$ is the decomposition coefficients of the field in the basis composed of the eigenvector of $\square_\perp$. Any electric field can be then represented in the modal basis $(k_x, k_y, \omega)$ in Cartesian coordinates, and $(k_r, l, \omega)$ in cylindrical coordinates.

***Galilean-transformed (uniform rectilinear motion) invariant wavepackets.*** The first example of invariant ST wavepackets are those propagating without any deformation in a frame propagating at their group velocity $v_g$. In this case, the transformation linking the field at a given propagation distance $z$ with the initial field is simply $t' \to t - z/v_g$. Finding the spatiotemporal wavepackets invariant under uniform rectilinear motion (and invariant under phase transformation), amounts to find the fields that belong to the kernel of the differential operator $\partial_z + K_1\partial_t - iK_0$, where $1/K_1$ is the group velocity of the built wavepacket and $K_0$ is its propagation constant. It immediately follows that the decomposition of rectilinear motion-invariant wavepackets only embeds eigenvectors whose eigenvalues respect:

$$K_z = K_0 + K_1\omega. \qquad (3)$$

One can now study how the mode-resolved spectrum of such invariant fields are structured in bulk media. For simplicity, we will consider the dispersive properties of the medium by means of the usual Taylor expansion around a given arbitrarily chosen frequency $\omega_0$ and up to the second-order dispersion coefficient. Now, Eq. 3 reads:

$$k_\perp^2 - \delta_2\Omega^2 - 2\delta_1\Omega - \delta_0 = 0, \qquad (4)$$

where $\Omega = \omega - \omega_0$, $k_0 = k(\Omega = 0)$, $k_1 = \partial_\omega k(\Omega = 0)$, $k_2 = \partial_\omega^2 k(\Omega = 0)$, $\delta_2 = (k_1^2 + k_0 k_2 - K_1^2)$, $\delta_1 = (k_0 k_1 - K_0 K_1)$, and $\delta_0 = (k_0^2 - K_0^2)$. The above algebraic expression in 3D-space refers to a quadric surface of dimension 2 (note that higher order terms in Ω have been neglected). Such quadrics are easily classified and named by their shape. Here the surface depends on the signs of $\delta_2$ and $\Delta = \delta_1^2 - \delta_2\delta_0$, and the considered coordinates system. Similar analysis for bulk media has been performed to define 2D conical waves.[38-39] Table 1 summarizes the distinct regimes and associated quadrics of rectilinear motion-invariant wavepackets. It reveals that the nature of quadrics is not fully driven by the considered dispersion regime (normal or anomalous).

| **Quadric surface** | $\boldsymbol{\delta_2}$ | $\Delta$ | **Coordinate system** |
|---|---|---|---|
| *Hyperboloid one sheet* | $> 0$ | $< 0$ | Cartesian |
| *Hyperboloid two sheets* | $> 0$ | $> 0$ | Cartesian |
| *Elliptic cone* | $> 0$ | $= 0$ | Cartesian |
| *Ellipsoid* | $< 0$ | $> 0$ | Cartesian |
| *Elliptic paraboloid* | $= 0$ | | Cartesian |
| *Paraboloid cylinder* | $= 0$ | | Cylindrical |
| *Hyperbolic cylinder* | $> 0$ | | Cylindrical |
| *Elliptic cylinder* | $< 0$ | $> 0$ | Cylindrical |

Table 1: Rectilinear motion-invariant wavepackets in bulk media.

- *Case 1: normal dispersion* ($k_2 > 0$).

In the normal dispersion regime, the common situation corresponds to $\delta_2 > 0$ ($K_1$ close to $k_1$). Figure 1(a-b) shows the corresponding surfaces for negative and positive values of $\Delta$ in Cartesian coordinates (i.e., in the $(k_x, k_y, \omega)$ space), namely hyperboloids of one or two sheets. When this term is null, we find an elliptic cone as shown in Fig. 1(c). As shown in subplots (a-c), the term $\Delta$ mainly governs the existence of involved frequencies around the central wavelength of the invariant ST wavepacket. This effect is also clearly visible on the limiting case of ST wave sheets [see conic sections defined as the intersection of the quadric with the plane $k_y = 0$ in Fig. 1(f-h)]. Such programmable correlations between the spatiotemporal degrees of freedom have recently been studied in detail.[25,30,40,41] Such waves take the forms of different hyperbola in the $(k_x, \omega)$ and $(k_x, K_z - k_0 - k_1\omega)$ planes with baseband or passband features, while the relation between $K_z$ and $\omega$ is simply linear, whose slope corresponds to the chosen group velocity. In those subplots, in the vicinity of conic sections, we also point out the local curvature of phase-matching induced by dispersion, in strong contrast to standard light cones[25,30,40,41] restricted to free-space propagation of narrowband wavepackets. Next, it is worth mentioning that the sign of parameter $\delta_2$ can become negative when $K_1 \gg k_1$. As a consequence, one can define a critical group velocity $1/K_1$ below which $\delta_2 < 0$, and we then retrieve the typical quadric surface usually obtained in the anomalous dispersion regime (i.e., an ellipsoid) investigated below. Finally, in the case of cylindrical coordinates, note that quadric surfaces [in the $(k_\perp, l, \omega)$ space] naturally embed the typical patterns of X-wave (or conical wave) solutions previously studied in bulk[28-29] or guiding[27,42] media, obtained as the intersection of the quadric surfaces and the plane defined by $l = 0$ (see Table 1).

- *Case 2: anomalous dispersion* ($k_2 < 0$).

In that dispersion regime, the common situation corresponds here to $\delta_2 < 0$. The associated quadric is an ellipsoid in Cartesian coordinates, as shown in Fig. 1(d) or an elliptic cylinder in cylindrical coordinates. In the latter case, one retrieves the typical signature of O-waves (light bullets) previously studied in bulk media[28-29]. Again, the limiting case of ST wave sheet can be obtained for $k_y = 0$ in Fig. 1(i). This wave takes the form of distinct ellipses in the $(k_x, \omega)$ and $(k_x, K_z - k_0 - k_1\omega)$ planes, while the linear relation between $K_z$ and $\omega$ is again driven by the chosen group velocity. As previously, the sign of parameter $\delta_2$ can nevertheless change by strongly varying $K_1$. Here, one can define a critical group velocity $1/K_1$ beyond which $\delta_2 > 0$, and the corresponding quadric becomes a hyperboloid (typical feature of normal dispersion regime above-studied).

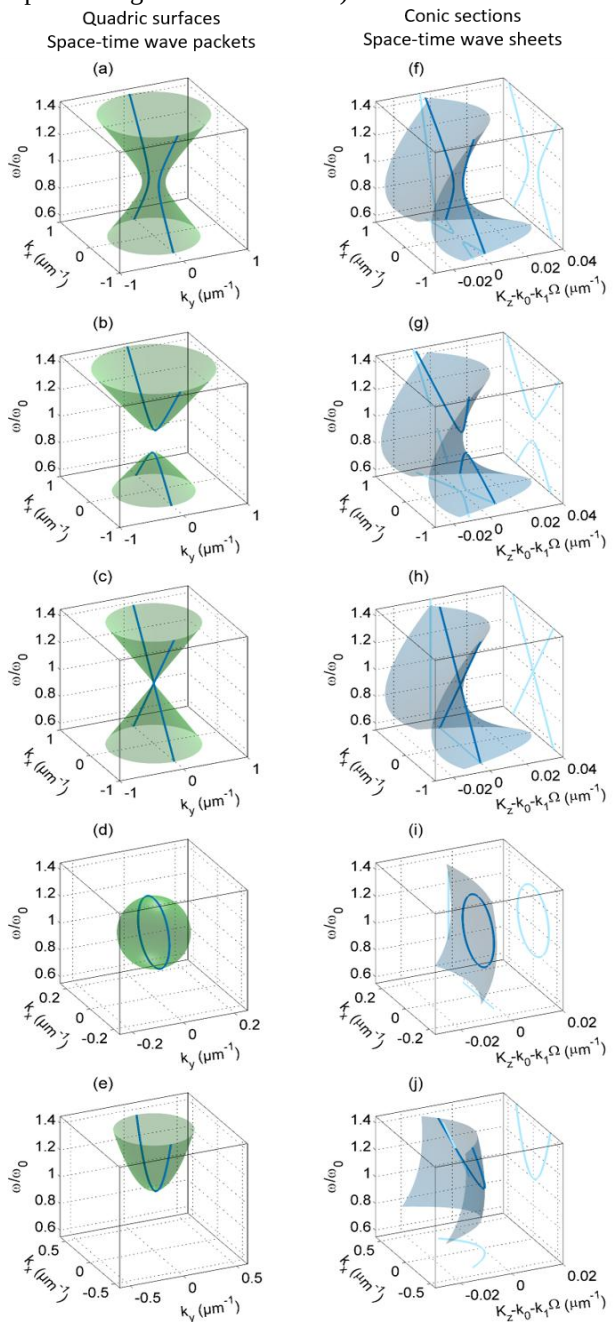


**Figure 1.** Quadrics governing (uniform rectilinear motion) invariant ST wavepacket in bulk fused silica. (a-c) Center wavelength at 800 nm in normal dispersion. (d-e) Center wavelength at 1600 nm in anomalous dispersion. (a) Hyperboloid of one sheet for $(k_0 - K_0) = 15$ cm$^{-1}$ and $(k_1 - K_1) = 4$ ps/m. (b) Hyperboloid of two sheets for $k_0 = K_0$ and $(k_1 - K_1) = 9$ ps/m. (c) Elliptic cone for $k_0 = K_0$ and $k_1 = K_1$. (d) Ellipsoid for $(k_0 - K_0) = 15$ cm$^{-1}$ and $k_1 = K_1$. (e) Elliptic paraboloid for $k_0 = K_0$ and $(k_1 - K_1) = 19.82$ ps/m. In

subplots (a-e), blue lines indicate the limiting case of space-time light sheets when $k_y = 0$. Corresponding conic sections are depicted in subplots (f-j) with their projections onto the distinct planes. Local curvatures induced by dispersion are mapped in the vicinity of conic sections.

Such cross-overs from one to another type of surfaces shows that, by carefully choosing $K_1$, one can easily overcome limitations in the design of ST wavepackets related to the dispersion of the medium under study.

Finally, a specific configuration of light structuring for invariant ST wavepackets is obtained when $\delta_2 = 0$, again whatever the dispersion regime. Equation (4) becomes linear in terms of frequencies Ω. The associated quadric of rank 2 is an elliptic paraboloid in Cartesian coordinates, as shown in Fig. 1(e) or a paraboloid cylinder in cylindrical coordinates. In the limiting case of ST wave sheet in Fig. 1(j), the conic section degenerates into a simple parabola.

***Galilean-transformed (uniform motion and rotation) invariant wavepackets.*** One can push further the classification of invariant ST wavepackets by noticing that rectilinear motion-invariant fields form a subgroup of the family which is not only invariant under uniform motion but also invariant at a given rotation around the $z$ axis. The latter, called spatiotemporal helicon wavepackets,[28] belong to the kernel of the space-time screw axis symmetry differential operator $\Pi = \partial_z + K_1\partial_t + K_l L_z - iK_0$, where $K_l$ is an arbitrarily chosen constant and $L_z = x\partial_y - y\partial_x = \partial_\theta$ is the z-component of the angular momentum operator. In the following, the study of ST helicon wavepackets is treated in the more general framework of cylindrically symmetric waveguides, i.e., in media whose refractive index $n$ may exhibit a radial dependence. The bulk case can then be seen as the limiting case of waveguide of infinite dimension.

For simplicity, we will restrict our study to a scalar approach by considering the weak guidance approximation. The partial differential equation driving the linear propagation of an electric field $E$ is then given in cylindrical coordinates by:

$$\left[\partial_z^2 + \partial_r^2 + \frac{1}{r}\partial_r + \frac{1}{r^2}\partial_\theta^2 + \frac{n^2(r,\omega)\omega^2}{c^2}\right]\tilde{E}(r,\theta,z,\omega) = 0, \quad (5)$$

where $n(r,\omega)$ is the radial-dependent refractive index at $\omega$. By using the separation of transverse and longitudinal variables, the linear evolution of the field along the propagation axis is given in the modal basis[35] by:

$$\partial_z \bar{E} = iK_z(l,p,\omega)\bar{E}, \quad (6)$$

where $K_z(l,p,\omega)$ is the propagation constant of the OAM mode $(l,p)$ at the frequency $\omega$. Recall that $l$ and $p$ refer here to azimuthal and radial indices, where $l(0,\pm1,\pm2,\pm3,\dots)$ is the topological charge, related to the phase front of OAM modes. The modes form an orthonormal basis so that any electric field $E$ can be expressed as

$$E(r,\theta,t) = \int \sum_{l,p} \bar{E}(l,p,\omega)\, A_{l,p}(r,\omega) e^{i(l\theta-\omega t)} d\omega, \quad (7)$$

where $A_{l,p}(r,\omega)$ is the transverse envelope of the mode $(l,p,\omega)$ and $\bar{E}(l,p,\omega)$ are the electric field coordinates in the modal basis. Looking for fields that belong to the kernel of Π immediately implies that the decomposition of such wavepackets only embeds a family of eigenvectors whose eigenvalues respect:

$$K_z(l,p,\omega_{lp}) = K_0 + K_1\omega_{lp} + K_l l. \quad (8)$$

Accordingly, any electric field built from a given family is a diffraction- and dispersion-free ST wavepacket propagating at the group velocity $1/K_1$ whose intensity continuously rotates around the propagation axis with a spatial period $2\pi/K_l$. Before studying how the mode-resolved spectrum of such invariant fields is structured in the modal space $(l,p,\omega)$, one has to emphasize that, generally speaking, the propagation constant in a waveguide (nonlinearly) depends on the topological charge $l$. Hence, still considering only second-order dispersion around a given arbitrarily chosen frequency $\omega_0$, the propagation constant of a waveguide can be well approximated as

$$K_z^2 \simeq \left(k_0 + k_1\Omega + \frac{k_2}{2}\Omega^2\right)^2 - \Gamma(l,p,\Omega), \quad (9)$$

with Γ is a three-dimensional second-order polynomial:

$$\begin{aligned}\Gamma(l,p,\Omega) = {} & \gamma_{0,0,0} + \gamma_{1,0,0}|l| + \gamma_{0,1,0}p + \gamma_{0,0,1}\Omega \\ & + \gamma_{2,0,0}l^2 + \gamma_{0,0,2}\Omega^2 + \gamma_{0,2,0}p^2 \\ & + \gamma_{1,1,0}|l|p + \gamma_{1,0,1}|l|\Omega + \gamma_{0,1,1}p\Omega\end{aligned}$$

where the coefficients $\gamma_{i,j,k}$ depend on the geometry of the considered waveguide. For the case of homogeneous bulk media, all coefficients vanish except $\gamma_{0,2,0}$ with $p$ being replaced by $k_r$.

Note that the propagation constant $K_z$ usually does not depend on the sign of $l$. This will have some consequences in the geometric nature of the surfaces describing spatiotemporal helicon wavepackets. Inserting Eq. 9 in Eq. 8, it follows that spatiotemporal helicon wavepackets are contained in surfaces whose algebraic expression are

$$\begin{aligned}\Gamma(l,p,\Omega) - \delta_2\Omega^2 + K_l^2 l^2 + 2K_1K_l\Omega l \\ -2\delta_1\Omega + 2K_0K_l l - \delta_0 = 0,\end{aligned} \quad (10)$$

First, since $\Gamma(l,p,\Omega)$ depends on $|l|$, it is straightforward to notice that the surface embedding spatiotemporal wavepackets will be composed of two different quadrics (one for $l > 0$ and another for $l < 0$). However, it appears that the rank and nature of the two involved quadrics is the same. The only difference between the two will be the

position of their respective principal axis. Then, it is sufficient to study the nature of the quadric for positive $l$ only. To this purpose, one has to study the associated matrix $M_Q$ to relation (10):

$$M_Q = \begin{pmatrix} \gamma_{2,0,0} + K_l^2 & \frac{\gamma_{1,1,0}}{2} & \frac{\gamma_{1,0,1}}{2} + K_1 K_l \\ \frac{\gamma_{1,1,0}}{2} & \gamma_{0,2,0} & \frac{\gamma_{0,1,1}}{2} \\ \frac{\gamma_{1,0,1}}{2} + K_1 K_l & \frac{\gamma_{0,1,1}}{2} & \gamma_{0,0,2} - \delta_2 \end{pmatrix} \quad (11)$$

The relative signs of the eigenvalues $(\lambda_1, \lambda_2, \lambda_3)$ of $M_Q$ completely classify the nature of the quadric surface in the frequency-resolved modal space.

As an example, we investigate below ST wave structures in a simple and analytical case at the frontier between bulk media and fibers, namely a dispersive medium of finite transversal dimension (radius $R$). Thus, the propagation constants can be simply described through $\Gamma(l, p, \Omega) = \alpha_{lp}^2 / R^2$, where $\alpha_{lp}$ is the $p^{th}$ root of $l^{th}$ Bessel function of first kind $J_l$. Using the formalism described above, with a second-order polynomial fit of $\alpha_{lp}^2$ (independent of $\Omega$), namely $\gamma_{2,0,0} = 1.438/R^2$, $\gamma_{0,2,0} = 9.864/R^2$, $\gamma_{0,0,2} = 0$, $\gamma_{1,1,0} = 9.893/R^2$, $\gamma_{1,0,1} = 0$, and $\gamma_{0,1,1} = 0$, one can find the following matrix $M_{Q,\mathrm{rod}}$:

$$M_{Q,\mathrm{rod}} = \begin{pmatrix} \frac{1.438}{R^2} + K_l^2 & \frac{9.893}{2R^2} & K_1 K_l \\ \frac{9.893}{2R^2} & \frac{9.864}{R^2} & 0 \\ K_1 K_l & 0 & -\delta_2 \end{pmatrix} \quad (12)$$

It appears that analytical formula for eigenvalues of such a matrix of the silica rod remains too complex to be presented here. However, in order to get a simple overview of the nature of quadrics, we considered small values of $K_l$. This allows to approximatively find the following eigenvalues:

$$\lambda_1 \simeq \frac{12.1}{R^2}, \lambda_2 \simeq -\frac{0.85}{R^2}, \lambda_3 = -\delta_2. \quad (13)$$

Accordingly, the quadric surface associated to ST helicon wavepackets in finite bulk media has a rank of 3 (unless $\delta_2 = 0$). Moreover, since $\lambda_1 \lambda_2 < 0$, the quadric surfaces for $l > 0$ and $l < 0$ are necessarily either one- or two-sheet hyperboloids or elliptic cones in this approximated framework. In the limiting case of (infinite) bulk media, one can easily find tractable analytical formula of eigenvalues from matrix associated to relation (10) with $\Gamma = k_r^2$.

In the general framework of matrix $M_{Q,\mathrm{rod}}$ (12), typical examples of quadrics are shown in Fig. 2(a-b) in both dispersion regimes. Note that for a clearer illustration, surfaces are plotted even if only discrete values can be found for parameters $(l, p, \omega)$. We confirm that for each configuration the global surface is composed of two different quadrics (one for $l > 0$ and another for $l < 0$), namely hyperboloids of one or two sheets. Discrete values are then shown for limited cases corresponding to conic sections when $l = 0$ or $p = 1$. In the limiting case of infinite bulk media, the quadrics involved for structuring ST helicon wavepackets are theoretically hyperboloids, however, in practice one eigenvalue tends to zero so that surfaces approaches an elliptic/hyperbolic paraboloid, depending on the respective value of $\delta_2$, see Fig. 2(c-d). Note that for $K_l = 0$, we retrieve an elliptic/hyperbolic cylinder as described in Table 1.

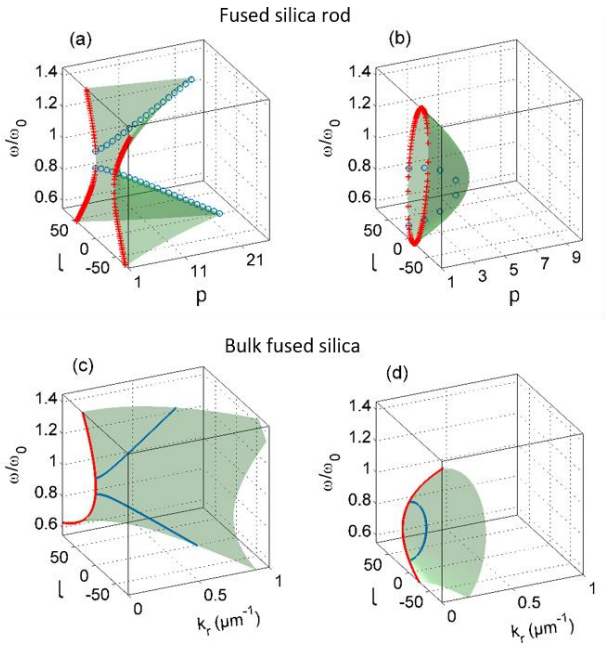


**Figure 2**. Examples of quadric surfaces (from Eq. 10) governing phasematching of space-time helicon wavepackets in a fused silica rod with radius $R = 100$ μm (a-b) and bulk fused silica (c-d). Subplots (a: Two hyperboloids of one sheet, c: hyperbolic paraboloid) correspond to the normal dispersion regime with central wavelength fixed at 800 nm, and $k_0 = K_0$, $(k_1 - K_1) = -4$ ps/m, $2\pi/K_l = 2$ cm. Subplots (b: Two hyperboloids of two sheets, d: elliptic paraboloid) correspond to the anomalous dispersion regime with central wavelength fixed at 1600 nm. $k_0 = K_0$, $(k_1 - K_1) = -12$ ps/m, and $2\pi/K_l = 1$ cm (6 cm in subplot d). Blue lines/circles indicate conic sections regarding the limiting cases of non-rotating space-time wavepackets (without superposed OAM) when $l = 0$. Red lines/crosses indicate the simple cases when $k_r = 0$ or $p = 1$.

***Numerical construction of wavepackets.*** Next, we present some examples illustrating our general approach of synthesizing rotating ST wavepackets through quadric phasematching of their spatiotemporal optical components (Eq. 10). In particular, we construct such ST wave structures in the simple case of a fused silica rod with

radius $R = 100$ µm, both in normal and anomalous dispersion regimes. As a result, for each couple $(l, p)$, one must find the roots of the quadric, thus corresponding to frequencies $\Omega_{lp}$ that depict the family of phase-matched modes $(l, p, \Omega_{lp})$. Figure 3(a) shows the overall three-dimensional pattern of phasematching obtained in the normal dispersion regime, when considering a central wavelength $\lambda_0 = 2\pi c/\omega_0 =$ 800 nm, and the arbitrary choice of the constants $K_1 = k_1$ and $K_0 = k_0$ (i.e., propagation constants of the wavepacket are those of $\omega_0$). The rotation period is here fixed equal to $2\pi/|K_l| = 1$ cm. The linear construction of a helicon wavepacket then results from the superposition of the calculated frequencies $\Omega_{lp}$. Figure 3(b) presents an example corresponding to a particular case of selected modes with various radial and angular indices $(0 \leq l \leq 8,$ and $1 \leq p \leq 8)$, and with equal spectral amplitudes and phases (see circles in Fig. 3a). The successive subplots display the isosurface of the spatiotemporal intensity at half-maximum at distinct propagation distances. The wavepacket looks like a corkscrew in space-time coordinates with extreme localization since all frequencies are in phase. It clearly reveals the spiraling trajectory of the intensity pattern while maintaining its initial distribution over propagation. This helicon wavepacket does not disperse and simply rotates during its propagation around the z- and t-axes because of its inherent invariant nature. The direction of rotation is driven by the sign of $K_l$. Note that complex engineered 3D-patterns can be obtained by a careful selection of multiple higher-order modes at the phase-matched discrete frequencies.

Another example of quadric phasematching obtained in the anomalous dispersion regime is shown in Fig. 3(c), when considering a central wavelength $\lambda_0 = 2\pi c/\omega_0 =$ 1800 nm, and the arbitrary choice of the constants $K_1 = k_1$ and $K_0 = k_0$. The rotation period is now fixed equal to $2\pi/|K_l| = 1.3$ cm. Figure 3(d) presents an example of constructed helicon wavepacket obtained from the superposition of modes with the following radial and angular indices: $-22 \leq l \leq 0$, and $1 \leq p \leq 2$, and with equal spectral amplitudes and phases (see circles in Fig. 3c). Again we retrieve the typical invariant spiraling trajectory of the intensity pattern. However, we here notice the more complex spatiotemporal pattern made of three consecutive high-intensity sub-pulses with distinct spatial arrangements.

***Discussion and conclusion.*** The concept of invariant ST wavepackets has emerged as a very promising and powerful tool for controlling the propagation dynamics of pulsed electromagnetic fields. By finely tailoring the modal distribution of the spectral components embedded, one can control in large extent both trajectory and velocity of ST wavepackets, but also the way they spread both in time and space, and this, whatever the dispersion regime. This degree of control let envision extremely exciting applications and new all-optical functionalities. Here, by invoking symmetry arguments, we have shown that invariant ST wavepackets refer to three-dimensional objects whose modal spectral distributions lie on quadrics surfaces.

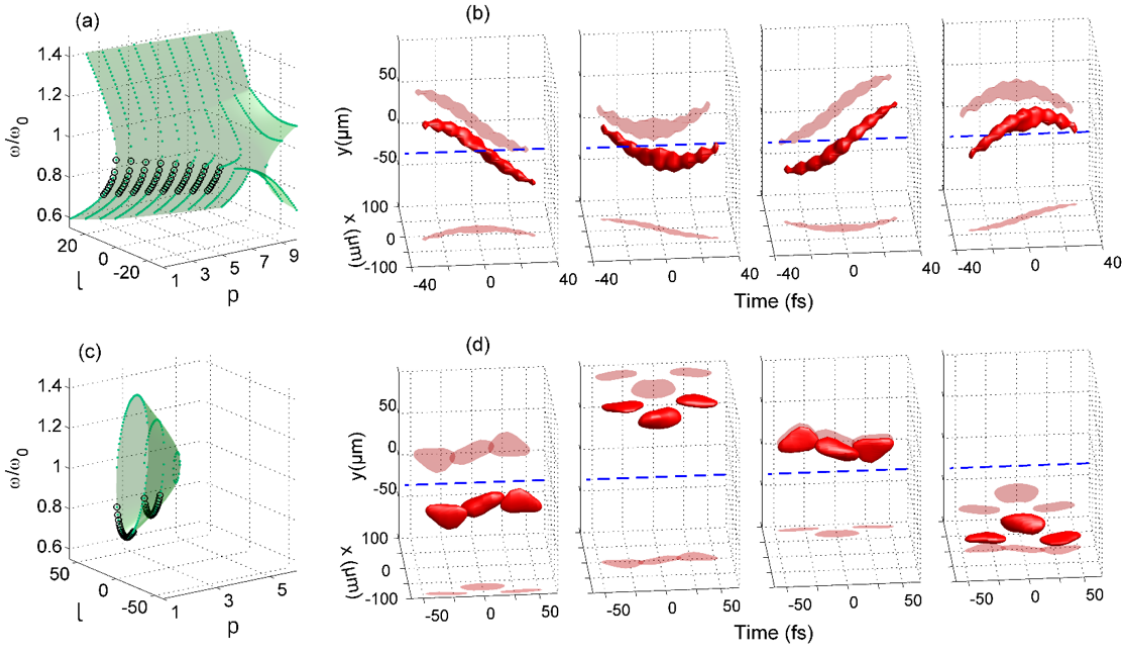

**Figure 3.** Examples of helicon wavepackets constructed from quadric phasematching of spatiotemporal components (from Eq. 10) in a fused silica rod with radius $R = 100$ µm. (a,c) Quadric surfaces obtained both in normal and anomalous dispersion regimes. Green dots indicate discretized conic sections for each $p$ coordinate. Black circles correspond to the selected modes used for the linear construction of helicon wavepackets depicted in (b,d) through iso-surfaces of their spatiotemporal intensity pattern at half-maximum. The successive subplots obtained every $\pi/(2|K_l|)$ confirm the invariant nature of helicon wavepackets over propagation. The dashed blue line indicates the origin $(x = 0, y = 0)$. Projections on planes (shadow plots) are also provided for a clear observation of rotation.

With the extremely rapid progresses made for manipulating ST wavepackets,[16,33] we hope this work will inspire a wealth of applications, such as recent 3D wavepackets with intriguing vortices and singularities,[17,43-44] and for which ST invariance feature would require further investigations. Beyond this simple but far-reaching concept of structured light for controlling the linear pulse propagation dynamics, note that the study of quadric waves, the general concept embedding conical waves, will also help in understanding the physics underlying the mechanism of supercontinua generation. For instance, a recent numerical work[35] has already reported that the supercontinuum generated by a helicon pulse is naturally structured in a quadric wave that respects the underlying symmetry imposed by the nonlinear propagation of the pump. Finally, the formalism of quadric phasematching is not limited to electromagnetic fields and could find applications in various branches of wave physics,[45-49] such as acoustics, polaritonics, plasma, gravity, and Bose condensate physics, in order to explore the dynamics of three-dimensional spiraling wavepackets with topological properties.

***Conflict of interest.*** The authors declare no competing financial interest.

***Funding Sources.*** The authors acknowledge support from French programs "Investments for the Future" operated by National Research Agency (ISITE-BFC, contract ANR-15-IDEX-03; EIPHI Graduate School, contract ANR-17-EURE-0002; EQUIPEX+ Smartlight, contract ANR-21-ESRE-0040), and from Région Bourgogne Franche-Comté.

## References

[1] E. P. Wigner, "Symmetry and conservation laws," Phys. Today **17**, 34 (1964).
[2] D. J. Gross, "The role of symmetry in fundamental physics," Proc. Natl. Acad. Sci. **10**, 14256 (1996).
[3] S. A. Khan, "Group theory in geometrical optics," Jpn. J. Appl. Phys. **17**, 161 (1978).
[4] A. J. Dragt, "Lie algebraic theory of geometrical optics and optical aberrations," J. Opt. Soc. Am.**72**, 372 (1982).
[5] C. P. Boyer, E. G. Kalnins, and W. Miller, Jr, "Symmetry and separation of variables for the Helmholtz and Laplace equations," Nagoya Math. J. **60**, 35 (1976).
[6] A. Wünsche, "Generalized Gaussian beam solutions of paraxial optics and their connection to a hidden symmetry," J. Opt. Soc. Am. A **6**, 1320 (1989).
[7] B. M. Rodríguez-Lara, R. El-Ganainy, and J. Guerrero, "Symmetry in optics and photonics: a group theory approach," Sci. Bull. **63**, 244 (2018).
[8] J. Durnin, "Exact solutions for nondiffracting beams. I. The scalar theory," J. Opt. Soc. Am. A **4**, 651 (1987).
[9] J. C. Gutiérrez-Vega, M. D. Iturbe-Castillo, and S. Chávez-Cerda, "Alternative formulation for invariant optical fields: Mathieu beams," Opt. Lett. **25**, 1493 (2000).
[10] M. A. Bandres and B. M. Rodríguez-Lara, "Nondiffracting accelerating waves: Weber waves and parabolic momentum," New J. Phys. **15**, 013054 (2013).
[11] Y. Shen, X. Wang, Z. Xie, C. Min, X. Fu, Q. Liu, M. Gong, and X. Yuan, "Optical vortices 30 years on: OAM manipulation from topological charge to multiple singularities," Light. Sci. Appl. **8**, 90 (2019).
[12] K. Y. Bliokh and F. Nori, "Spatiotemporal vortex beams and angular momentum," Phys. Rev. A **86**, 033824 (2012).
[13] A. Chong, C. Wan, J. Chen, and Q. Zhan, "Generation of spatiotemporal optical vortices with controllable transverse orbital angular momentum," Nat. Photonics **14**, 350 (2020).
[14] S. W. Hancock, S. Zahedpour, A. Goffin, and H. M. Milchberg, "Free-space propagation of spatiotemporal optical vortices," Optica **6**, 1547 (2019).
[15] S.W. Hancock, S. Zahedpour, and H. M. Milchberg, "Mode structure and orbital angular momentum of spatiotemporal optical vortex pulses," Phys. Rev. Lett. **127**, 193901 (2021).
[16] Q. Cao, J. Chen, K. Lu, C. Wan, A. Chong, and Q. Zhan, "Non-spreading Bessel spatiotemporal optical vortices," Sci. Bull. **67**, 133 (2022).
[17] C. Wan, J. Chen, A. Chong, and Q. Zhan, "Photonic orbital angular momentum with controllable orientation," Natl. Sci. Rev., nwab149 (2021).
[18] H. Rubinsztein-Dunlop et al., "Roadmap on structured light," J. Opt. **19**, 013001 (2017).
[19] A. Forbes, M. de Oliveira, and M. R. Dennis, "Structured light," Nat. Photon. **15**, 253 (2021).
[20] M. Piccardo et al., "Roadmap on multimode light shaping," J. Opt. **24,** 013001 (2022).
[21] S. M. Lloyd, M. Babiker, G. Thirunavukkarasu, and J. Yuan, "Electron vortices: Beams with orbital angular momentum," Rev. Mod. Phys. **89**, 035004 (2017).

[22] M. Urrutia and R. L. Stenzel, "Helicon waves in uniform plasmas. IV. Bessel beams, Gendrin beams, and helicons", Phys. Plasmas **23**, 052112 (2016).
[23] K. Y. Bliokh and F. Nori, "Spin and orbital angular momenta of acoustic beams," Phys. Rev. B **99**, 174310 (2019).
[24] G. M. Vanacore, G. Berruto, I. Madan, E. Pomarico, P. Biagioni, R. J. Lamb, D. McGrouther, O. Reinhardt, I. Kaminer, B. Barwick, H. Larocque, V. Grillo, E. Karimi, F. J. García de Abajo, and F. Carbone, "Ultrafast generation and control of an electron vortex beam via chiral plasmonic near fields," Nat. Materials **18**, 573 (2019).
[25] H. E. Kondakci and A. F. Abouraddy, "Diffraction-free space-time light sheets," Nat. Photon. **11**, 733 (2017).
[26] K. J. Parker and M. A. Alonso, "Longitudinal iso-phase condition and needle pulses," Opt. Express **24**, 28669 (2016).
[27] B. Kibler and P. Béjot, "Discretized conical waves in multimode optical fibers," Phys. Rev. Lett. **126**, 023902 (2021).
[28] D. Faccio, A. Couairon, and P. Di Trapani, *Conical Waves, Filaments and Nonlinear Filamentation Optics* (Aracne, Roma, 2007).
[29] H. E. Hernandez-Figueroa, M. Zamboni-Rached, and E. Recami, *Localized Waves* (Wiley, Hoboken, 2008).
[30] H. E. Kondakci and A. F. Abouraddy, "Optical space-time wave packets having arbitrary group velocities in free space," Nat. Commun. **10**, 929 (2019).
[31] M. Yessenov, L.A. Hall, and A.F. Abouraddy, "Engineering the Optical Vacuum: Arbitrary Magnitude, Sign, and Order of Dispersion in Free Space Using Space−Time Wave Packets", ACS Phot. **8**, 2274-2284 (2021).
[32] L. A. Hall and A. F. Abouraddy, "Canceling and inverting normal and anomalous group-velocity dispersion using space-time wave packets," arXiv:2202.01148, https://doi.org/10.48550/arXiv.2202.01148.
[33] M. Yessenov, J. Free, Z. Chen, E. G. Johnson, M. P. J. Lavery, M. A. Alonso, and A. F. Abouraddy, "Space-time wave packets localized in all dimensions," arXiv:2111.03095, https://doi.org/10.48550/arXiv.2111.03095.
[34] M. Kolesik, E. M. Wright, and J. V. Moloney, "Interpretation of the spectrally resolved far field of femtosecond pulses propagating in bulk nonlinear dispersive media," Opt. Express **13**, 10729-10741 (2005).
[35] P. Béjot and B. Kibler, "Spatiotemporal Helicon Wavepackets", ACS Phot. **8**, 2345-2354 (2021).
[36] C. Guo, M. Xiao, M. Orenstein, and S. Fan, "Structured 3D linear space–time light bullets by nonlocal nanophotonics", Light Sci. Appl. **10**, 160 (2021).
[37] M. S. Mills, G. A. Siviloglou, N. Efremidis, T. Graf, E. M. Wright, J. V. Moloney, and D. N. Christodoulides, "Localized waves with spherical harmonic symmetries," Phys. Rev. A **86**, 063811 (2012).
[38] S. Malaguti, G. Bellanca, and S. Trillo, "Two-dimensional envelope localized waves in the anomalous dispersion regime," Opt. Lett. **33**, 1117 (2008).
[39] S. Malaguti and S. Trillo, "Envelope localized waves of the conical type in linear normally dispersive media," Phys. Rev. A **79**, 063803 (2009).
[40] B. Bhaduri, M. Yessenov, and A. F. Abouraddy, "Anomalous refraction of optical spacetime wave packets," Nat. Photon. **14**, 416 (2020).
[41] M. Yessenov, B. Bhaduri, H. E. Kondakci, and A. F. Abouraddy, "Classification of propagation-invariant space-time wave packets in free space: Theory and experiments," Phys. Rev. A **99**, 023856 (2019).
[42] K. Tarnowski, S. Majchrowska, P. Béjot, and Bertrand Kibler, "Numerical modelings of ultrashort pulse propagation and conical emission in multimode optical fibers", J. Opt. Soc. Am. B **38**, 732-742 (2021)
[43] J. Chen, C. Wan, A. Chong, and Q. Zhan, "Experimental demonstration of cylindrical vector spatiotemporal optical vortex," Nanophotonics **10**, 4489-4495 (2021).
[44] C. Wan, Q. Cao, J. Chen, A. Chong, and Q. Zhan, "Photonics toroidal vortex," arXiv:2109.02833, https://doi.org/10.48550/arXiv.2109.02833.
[45] T. Brunet, J-L. Thomas, R. Marchiano, and F. Coulouvrat, "Experimental observation of azimuthal shock waves on nonlinear acoustical vortices," New J. Phys. **11**, 013002 (2009).
[46] L. Dominici, D. Colas, A. Gianfrate, A. Rahmani, V. Ardizzone, D. Ballarini, M. De Giorgi, G. Gigli, F. P. Laussy, D. Sanvitto, and N. Voronova, "Full-Bloch beams and ultrafast Rabi-rotating vortices," Phys. Rev. Res. **3**, 013007 (2021).
[47] J. Vieira, J. T. Mendonça, and F. Quéré, "Optical control of the topology of laser-plasma accelerators," Phys. Rev. Lett. **121**, 054801 (2018).
[48] J. Pierce, J. Webste, H. Larocque, E. Karimi, B. McMorran, and A. Forbes, "Coiling free electron matter waves," New J. Phys. **21**, 043018 (2019).
[49] F. A. Asenjo and S. A. Hojman, "Nondiffracting gravitational waves", Eur. Phys. J. C **81**, 81-98 (2021).